

Detection of large scale intrinsic ellipticity-density correlation from the Sloan Digital Sky Survey and implications for weak lensing surveys

Rachel Mandelbaum^{1*}, Christopher M. Hirata^{1,2}, Mustapha Ishak^{3,4},
Uroš Seljak^{1,5}, and Jonathan Brinkmann⁶

¹*Department of Physics, Jadwin Hall, Princeton University, Princeton, NJ 08544, USA*

²*Institute for Advanced Study, Einstein Drive, Princeton, NJ 08540, USA*

³*Department of Astrophysical Sciences, Princeton University, Princeton, NJ 08544, USA*

⁴*Department of Physics, The University of Texas at Dallas, Richardson TX 75083, USA*

⁵*International Centre for Theoretical Physics, Strada Costiera 11, 34014 Trieste, Italy*

⁶*Apache Point Observatory, 2001 Apache Point Road, Sunspot NM 88349, USA*

25 August 2018

ABSTRACT

The power spectrum of weak lensing shear caused by large-scale structure is an emerging tool for precision cosmology, in particular for measuring the effects of dark energy on the growth of structure at low redshift. One potential source of systematic error is intrinsic alignments of ellipticities of neighbouring galaxies (II correlation) that could mimic the correlations due to lensing. A related possibility pointed out by Hirata and Seljak (2004) is correlation between the intrinsic ellipticities of galaxies and the density field responsible for gravitational lensing shear (GI correlation). We present constraints on both the II and GI correlations using 265 908 spectroscopic galaxies from the Sloan Digital Sky Survey (SDSS), and using galaxies as tracers of the mass in the case of the GI analysis. The availability of redshifts in the SDSS allows us to select galaxies at small radial separations, which both reduces noise in the intrinsic alignment measurement and suppresses galaxy-galaxy lensing (which otherwise swamps the GI correlation). While we find no detection of the II correlation, our results are nonetheless statistically consistent with recent detections found using the SuperCOSMOS survey. Extrapolation of these limits to cosmic shear surveys at $z \sim 1$ suggests that the II correlation is unlikely to have been a significant source of error for current measurements of σ_8 with ~ 10 per cent accuracy, but may still be an issue for future surveys with projected statistical errors below the one per cent level unless eliminated using photometric redshifts. In contrast, we have a clear detection of GI correlation in galaxies brighter than L_* that persists to the largest scales probed ($60 h^{-1}\text{Mpc}$) and with a sign predicted by theoretical models. This correlation could cause the existing lensing surveys at $z \sim 1$ to underestimate the linear amplitude of fluctuations by as much as 20 per cent depending on the source sample used, while for surveys at $z \sim 0.5$ the underestimation may reach 30 per cent. The GI contamination is dominated by the brightest galaxies, possibly due to the alignment of brightest cluster galaxies (BCGs) with the cluster ellipticity due to anisotropic infall along filaments, although other sources of contamination cannot be excluded at this point. We propose that cosmic shear surveys should consider rejection of BCGs from their source catalogs as a test for GI contamination. Future high precision weak lensing surveys must develop methods to search for and remove this contamination if they are to achieve their promise.

Key words: cosmology: observations – gravitational lensing – large-scale structure of Universe.

1 INTRODUCTION

Weak gravitational lensing of distant galaxies has emerged as a powerful method for directly mea-

* Electronic address: rmandelb@princeton.edu

asuring the matter distribution in the universe (e.g. Mellier 1999; Bartelmann & Schneider 2001; Refregier 2003a) following detection of the two-point function of the lensing-induced shear by several groups (Bacon et al. 2000; Van Waerbeke et al. 2000; Rhodes et al. 2001; Hoekstra et al. 2002; Van Waerbeke et al. 2002; Brown et al. 2003; Jarvis et al. 2003). Also, weak lensing has been shown to be a very promising tool for precision cosmology (Hu 2002; Huterer 2002; Abazajian & Dodelson 2003; Benabed & Van Waerbeke 2004; Bernstein & Jain 2004; Ishak et al. 2004; Ishak 2005; Song & Knox 2005; Tereno et al. 2005; Upadhye et al. 2005), and has the clear advantage of being the simplest of the low-redshift cosmological probes to understand theoretically, since it is sensitive primarily to the dark matter whose interactions are described purely by gravity. Thus, most of the potential systematic errors in weak lensing are observational, i.e. associated with attempts to measure a small signal, in contrast with galaxy surveys, where large amounts of information are “lost” on quasilinear or nonlinear scales because of the lack of a robust prediction.

Examples of the observational systematics in weak lensing include uncertainties in the point-spread function (PSF) of the telescope, errors in correcting the ellipticity of a source galaxy for the PSF effects, star-galaxy separation, selection biases, deblending errors, detector nonlinearities, and noise-related biases. The list is long, and much of the effort by the weak lensing observers in the past several years has been devoted to these issues (Kaiser 2000; Erben et al. 2001; Bernstein & Jarvis 2002; Hirata & Seljak 2003a; Vale et al. 2004; Van Waerbeke et al. 2005). Nevertheless, it is important to remember that there are astrophysical uncertainties associated with weak lensing. Some of these, such as the error in N -body simulations or baryonic cooling effects, are limited to small scales only and are likely to be reduced significantly as the simulations improve (White 2004). Another astrophysical uncertainty is the redshift distribution dN/dz of the source galaxies. At least at the brighter magnitudes, these can be determined via spectroscopic redshifts (Bernstein & Jain 2004; Ishak & Hirata 2005; Ma et al. 2005), and at all magnitudes the distributions can be tested by comparing the galaxy-galaxy lensing signal among different source samples (Mandelbaum et al. 2005a; Huterer et al. 2005). Future low-frequency radio surveys may also open up the possibility of obtaining redshifts on many galaxies from the H I 21 cm line (e.g. Rawlings et al. 2004). In short, while the redshift distribution problem is not solved, there is no fundamental impediment to an accurate determination of dN/dz .

The final major astrophysical contaminant of weak lensing may be intrinsic alignments, i.e. correlations of the galaxy ellipticities with each other or with the density field. These correlations violate the usual assumption in lensing shear surveys that the source galaxies are randomly oriented so that any correlation between the apparent ellipticities of distinct objects is due to lensing. The purpose of this paper is to provide an observational constraint on these types of intrinsic alignments, and then to assess the implied contamination of upcoming cosmic shear surveys.

There are two types of intrinsic alignments that can contaminate the cosmic shear power spectrum, namely the intrinsic ellipticity-intrinsic ellipticity (II) correlation and

the gravitational shear-intrinsic ellipticity (GI) correlation. The II contamination is the easier to understand: it results from the possibility that two source galaxies are physically near each other and have correlated intrinsic ellipticities. This effect contributes an additive bias to any two-point shear statistic, though as pointed out by King & Schneider (2002) and Heymans & Heavens (2003), its effects can be minimized by using photometric redshifts to cross-correlate the shapes of galaxies at different redshifts. The GI contamination results from the possibility that, given two source galaxies, one is in front of the other. In this case, the intrinsic ellipticity of the nearby galaxy may be correlated with the density field that lenses the more distant galaxy, thus yielding a spurious contribution to the shear two-point function (Hirata & Seljak 2004). This contribution cannot be eliminated by selecting galaxies at different redshifts as for the II contamination, and in fact doing so will tend to increase any GI contamination.

So far, the main methods used to estimate the intrinsic alignments and assess their implications for cosmic shear have been theoretical results (analytical or simulation-based) and observations of low-redshift galaxies for which cosmic shear is negligible and any observed correlations must be intrinsic. Both methods have their limitations: the theory of galaxy alignments is subject to all of the uncertainties involved in the theory of galaxy formation, whereas the observations must be extrapolated from observable redshifts $z \sim 0.1$ to the redshifts $z \sim 1$ of the source galaxies used for lensing. Nevertheless, the theoretical predictions vary by more than an order of magnitude for II (Croft & Metzler 2000; Heavens et al. 2000; Lee & Pen 2000, 2001; Catelan et al. 2001; Crittenden et al. 2001; Jing 2002), so there is a clear role for observations in distinguishing which of these models is correct. The theory of GI correlations is even more rudimentary: only simple analytical models exist (Hui & Zhang 2002; Hirata & Seljak 2004).

At present, the most statistically powerful constraint on II correlations comes from the SuperCOSMOS data (Brown et al. 2002), which were re-analyzed by Heymans et al. (2004) with the conclusion that the II correlations are smaller than most of the theoretical predictions. The Sloan Digital Sky Survey (SDSS) is ideally suited to improving upon SuperCOSMOS because of the availability of spectroscopic redshifts, which allows for measurement of the correlations only between galaxies that are near each other in three-dimensional space, without the “noise” introduced by pairs of physically unassociated galaxies that happen to lie along the same line of sight. One can also attempt to constrain the GI correlation using low-redshift surveys such as SDSS. The GI correlation is essentially a measure of the correlation between the intrinsic ellipticities and the matter density; on sufficiently large scales, one can use the correlation between the intrinsic ellipticities and the galaxy density as a proxy. In this case the measurement of the GI correlation is model-dependent; however, we will argue that on large scales the associated uncertainty is probably less than the uncertainty associated with extrapolation to high redshift. The ability of spectroscopic redshifts to isolate pairs of galaxies at the same redshift is valuable for GI correlation studies to reduce noise, just as for II. It also enables us to cleanly separate GI from the “spurious” (for this work!)

density-ellipticity correlations caused by galaxy-galaxy lensing.

We note that there have been several observational studies of intrinsic alignments that were not motivated by potential contamination of cosmic shear measurements. These include Bernstein & Norberg (2002) and Hirata et al. (2004), who were interested in intrinsic alignment contamination of galaxy-galaxy lensing; Pen et al. (2000), Lee & Pen (2001), and Lee & Pen (2002), who were interested in using the tidal influence on intrinsic alignments to reconstruct the matter density field; and Navarro et al. (2004), who were interested in the formation of disk galaxies. These results are difficult (or, in some cases, impossible) to interpret in the context of cosmic shear because they are made at too small a physical scale, use measures of the galaxy shape not easily related to ellipticity, measure higher-order moments instead of density-ellipticity or ellipticity-ellipticity two-point functions, have complicated selection criteria that differ dramatically from those relevant to cosmic shear, or do not provide sufficient characterization of statistical errors.

The outline of the paper is as follows. We begin by introducing the formalism used in this paper in §2. The SDSS data used for this analysis is described in §3. We describe the calculation of the relevant correlation functions and show the resulting signal in §4. In §5 we use the computed signal to derive estimates of the contamination due to intrinsic alignments in current and future surveys. After proposing an explanation for the detected signal in §6, we conclude with a discussion of the implications of our results, and suggestions for future work.

Here we note the cosmological model and units adopted for this work. Pair separations are measured in comoving h^{-1} Mpc, with the angular diameter distance computed in a flat Λ CDM cosmology with $\Omega_m = 0.3$, $\Omega_\Lambda = 0.7$.

2 FORMALISM

The formalism for the analysis of the lensing shear two-point function (Miralda-Escudé 1991) and the intrinsic alignment contamination is well developed. We will briefly summarize the important equations here, and then define some new variables that relate to observables in galaxy surveys. Our notation is consistent with that of Hirata & Seljak (2004).

The observed shear γ of a galaxy is a sum of two components: the gravitational lensing-induced shear γ^G , and the “intrinsic shear” γ^I , which includes any non-lensing shear, typically due to local tidal fields. Therefore the E -mode shear power spectrum between any two redshift bins α and β is the sum of the gravitational lensing power spectrum (GG), the intrinsic-intrinsic, and the gravitational-intrinsic terms,

$$C_L^{EE}(\alpha\beta) = C_L^{EE,GG}(\alpha\beta) + C_L^{EE,II}(\alpha\beta) + C_L^{EE,GI}(\alpha\beta). \quad (1)$$

The pure gravitational lensing term is given by the Limber integral

$$C_L^{EE,GG}(\alpha\beta) = \int \frac{W_\alpha(\chi)W_\beta(\chi)}{\sin_K^2 \chi} P_\delta(L \csc_K \chi, \chi) d\chi, \quad (2)$$

where χ is the comoving distance of the lensing screen, P_δ is

the matter power spectrum, and the modified trigonometric functions are defined by

$$\sin_K \chi = \begin{cases} R_0 \sinh\left(\frac{\chi}{R_0}\right), & \Omega_K > 0, R_0 = \frac{c}{H_0\sqrt{\Omega_K}} \\ \chi, & \Omega_K = 0 \\ R_0 \sin\left(\frac{\chi}{R_0}\right), & \Omega_K < 0, R_0 = \frac{c}{H_0\sqrt{|\Omega_K|}} \end{cases} \quad (3)$$

and analogously for $\cos_K \chi$. The window function for redshift bin α is

$$W_\alpha(\chi) = \frac{3}{2}\Omega_m H_0^2 (1+z) \sin_K^2 \chi \times \int f_\alpha(\chi') (\cot_K \chi - \cot_K \chi') d\chi'. \quad (4)$$

Here $f_\alpha(\chi') = dn_\alpha/d\chi'$ is the distribution of comoving source distances for source sample α , and is equivalent to the redshift distribution if one fixes the homogeneous cosmology $\chi(z)$. The intrinsic alignment power spectrum is

$$C_L^{EE,II}(\alpha\beta) = \int \frac{f_\alpha(\chi)f_\beta(\chi)}{\sin_K^2 \chi} P_{\tilde{\gamma}^I}^{EE}(L \csc_K \chi, \chi) d\chi. \quad (5)$$

Here we have introduced the density-weighted intrinsic shear $\tilde{\gamma}^I = (1 + \delta_g)\gamma^I$, where δ_g is the galaxy (not matter!) overdensity $\rho_g/\bar{\rho}_g - 1$, and its E -mode power spectrum $P_{\tilde{\gamma}^I}^{EE}$. The GI or “interference” term is

$$C_L^{EE,GI}(\alpha\beta) = \int \frac{W_\alpha(\chi)f_\beta(\chi)}{\sin_K^2 \chi} P_{\delta,\tilde{\gamma}^I}(L \csc_K \chi) d\chi + (\alpha \leftrightarrow \beta). \quad (6)$$

To first order in the deflection angle, there is no B -mode induced by gravitational lensing shear. In this case, the B -mode power spectrum contains only a contribution from the intrinsic alignments,

$$C_L^{BB}(\alpha\beta) = C_L^{BB,II}(\alpha\beta) = \int \frac{f_\alpha(\chi)f_\beta(\chi)}{\sin_K^2 \chi} P_{\tilde{\gamma}^I}^{BB}(L \csc_K \chi, \chi) d\chi. \quad (7)$$

There are lensing-induced contributions to the B -mode shear from other effects, such as multiple deflections (Cooray & Hu 2002; Hirata & Seljak 2003b; Cooray et al. 2005) and, on small scales, modulation of the effective source redshift by galaxy clustering (Schneider et al. 2002).

Hirata & Seljak (2004) provided formulas relating the power spectra in Eqs. (2)–(7) to the real-space correlation functions. These formulas will be extremely useful because we directly measure the correlation functions in SDSS.¹ If one chooses any two points in the SDSS survey, their separation in redshift space can then be identified by the transverse separation r_p and the radial redshift space separation Π .² The + and \times components of the shear are measured with respect to the axis connecting the two galaxies (i.e. positive + shear is radial, whereas negative + shear is tangential). Then one can write the density-intrinsic shear correlation as

¹ We chose to measure the correlation function rather than the power spectrum simply because this involved minimal modification of pre-existing and well-tested code.

² The redshift space separation is frequently denoted π ; we use Π to avoid confusion since the number $\pi = 3.14\dots$ appears frequently in this paper.

$$P_{\delta, \tilde{\gamma}_I}(k) = -2\pi \int \xi_{\delta+}(r_p, \Pi) J_2(kr_p) r_p dr_p d\Pi, \quad (8)$$

where $\xi_{\delta+}(r_p, \Pi)$ is the correlation function between δ and $\tilde{\gamma}_+$. The intrinsic-intrinsic correlations are

$$P_{\tilde{\gamma}_I}^{EE}(k) = \int [\xi_{++}(r_p, \Pi) J_+(kr_p) + \xi_{\times\times}(r_p, \Pi) J_-(kr_p)] \times 2\pi r_p dr_p d\Pi \quad (9)$$

and

$$P_{\tilde{\gamma}_I}^{BB}(k) = \int [\xi_{++}(r_p, \Pi) J_-(kr_p) + \xi_{\times\times}(r_p, \Pi) J_+(kr_p)] \times 2\pi r_p dr_p d\Pi, \quad (10)$$

where $J_{\pm}(x) \equiv [J_0(x) \pm J_4(x)]/2$, and ξ_{++} and $\xi_{\times\times}$ represent correlation functions of $\tilde{\gamma}_I$. The existence of the Π integral suggests the definitions

$$w_{\delta+}(r_p) = \int_{-\infty}^{+\infty} \xi_{\delta+}(r_p, \Pi) d\Pi, \quad (11)$$

and similarly for w_{++} and $w_{\times\times}$.

3 DATA

The data used here are obtained from the SDSS. The SDSS (York et al. 2000) is an ongoing survey to image approximately π steradians of the sky, and follow up approximately one million of the detected objects spectroscopically (Eisenstein et al. 2001; Strauss et al. 2002; Richards et al. 2002). The imaging is carried out by drift-scanning the sky in photometric conditions (Hogg et al. 2001; Ivezić et al. 2004), in five bands (*ugriz*) (Fukugita et al. 1996; Smith et al. 2002) using a specially designed wide-field camera (Gunn et al. 1998). These imaging data are the source of the LSS sample that we use in this paper. In addition, objects are targeted for spectroscopy using these data (Blanton et al. 2003a) and are observed with a 640-fiber spectrograph on the same telescope (Gunn et al. 2005). All of these data are processed by completely automated pipelines that detect and measure photometric properties of objects, and astrometrically calibrate the data (Lupton et al. 2001; Pier et al. 2003; Tucker et al. 2005). The SDSS is well underway, and has had five major data releases (Stoughton et al. 2002; Abazajian et al. 2003, 2004, 2005; Finkbeiner et al. 2004; Adelman-McCarthy et al. 2005). This analysis uses the spectroscopically observed galaxies in the Value-Added Galaxy Catalog, LSS sample 14 (VAGC; Blanton et al. 2005), comprising 3423 square degrees with SDSS spectroscopic coverage.

3.1 Galaxy subsamples

In order to determine the correlation functions $\xi_{\delta+}$, ξ_{++} , and $\xi_{\times\times}$, one needs a sample of galaxies with which to measure the intrinsic shear, and a sample of galaxies with which to trace the density field. For this paper, we use only the SDSS spectroscopic galaxies, divided further into luminosity subsamples by absolute magnitude in the r filter. The four subsamples are described in Table 1. These are the

same as the L3–L6 subsamples used in the weak lensing analysis of Seljak et al. (2005a), and are very similar to the L4–L7 subsamples used in the galaxy power spectrum analysis of Tegmark et al. (2004).³ The absolute magnitude cuts are defined in terms of $h = H_0/(100 \text{ km s}^{-1} \text{ Mpc}^{-1})$ such that one can implement the cuts without specifying the value of H_0 . The magnitudes have been corrected for extinction, K -correction, and evolution. The extinction correction uses the Schlegel et al. (1998) dust reddening maps, with the extinction-to-reddening ratios given in Stoughton et al. (2002). The K -correction to $z = 0.1$ is performed using the `KCORRECT v1.11` software as described by Blanton et al. (2003b). The luminosities are corrected for passive evolution to $z = 0.1$ assuming constant $dM_r/dz = -1.6$, as in Blanton et al. (2003a). We exclude galaxies lying inside the bright star mask. Random catalogs were generated taking into account the variation of spectroscopic completeness with position. The random points were assigned absolute magnitudes drawn from a distribution consistent with the real sample, and random redshifts were assigned for a given magnitude given the selection function $\phi(M|z)$ from Blanton et al. (2003c). The sample selection criteria in this work and in that one are sufficiently similar that when $\phi(M|z)$ from that work is used to generate random redshifts, their probability distribution matches the redshift distribution of the real lenses used in this work (within the noise). Shape measurements were obtained via re-Gaussianization for 96 per cent of this sample (see §3.2); the remainder failed due various problems, such as interpolated or saturated centers.

3.2 Ellipticity data

In addition to a sample of galaxies, we also need their ellipticities. For this purpose, we use the measurements by Mandelbaum et al. (2005a), who obtained shapes for more than 30 million galaxies in the SDSS imaging data down to magnitude $r = 21.8$ (i.e. far fainter than the spectroscopic limit of the SDSS). This section briefly describes the RE-GLENS pipeline presented in Mandelbaum et al. (2005a), and the one modification we made for this paper.

The RE-GLENS pipeline obtains galaxy images in the r and i filters from the SDSS “atlas images” (Stoughton et al. 2002). The basic principle of shear measurement using these images is to fit a Gaussian profile with elliptical isophotes to the image, and define the components of the ellipticity

$$(e_+, e_{\times}) = \frac{1 - (b/a)^2}{1 + (b/a)^2} (\cos 2\phi, \sin 2\phi), \quad (12)$$

where b/a is the axis ratio and ϕ is the position angle of the major axis. The ellipticity is then an estimator for the shear,

$$(\gamma_+, \gamma_{\times}) = \frac{1}{2\mathcal{R}} \langle (e_+, e_{\times}) \rangle, \quad (13)$$

³ The Tegmark et al. (2004) sample differs in that a redshift cut was imposed to make the sample volume-limited, which simplified their analysis. Also, the Tegmark et al. (2004) subsample numbering is different: their L4 is similar to our L3, their L5 to our L4, etc. Finally, both the Tegmark et al. (2004) and the Seljak et al. (2005a) samples included a slightly stricter apparent magnitude cut than the sample in this work.

Table 1. The luminosity subsamples used in this analysis. The number of galaxies in each sample does not include failures. The linear bias is from Tegmark et al. (2004) and Seljak et al. (2005a), normalized to $\sigma_8 = 0.9$. The “total” linear bias and $\langle z \rangle$ are the number-weighted averages of the other samples.

Subsample	Magnitude range	Number of galaxies	Number of failures	Linear bias	$\langle z \rangle$
L3	$-20 \leq M_r + 5 \log_{10} h < -19$	66 312	2 723	0.85	0.07
L4	$-21 \leq M_r + 5 \log_{10} h < -20$	118 618	4 601	0.94	0.11
L5	$-22 \leq M_r + 5 \log_{10} h < -21$	73 041	2 829	1.08	0.15
L6	$-23 \leq M_r + 5 \log_{10} h < -22$	7 937	307	1.59	0.21
Total		265 908	10 460	0.98	0.12

where $\mathcal{R} \approx 0.87$ is called the “shear responsivity” and represents the response of the ellipticity (Eq. 12) to a small shear (Kaiser et al. 1995; Bernstein & Jarvis 2002). In practice, a number of corrections need to be applied to obtain the ellipticity. The most important of these is the correction for the smearing and circularization of the galactic images by the PSF; Mandelbaum et al. (2005a) uses the PSF maps obtained from stellar images by the PSP pipeline (Lupton et al. 2001), and corrects for these using the re-Gaussianization technique of Hirata & Seljak (2003a), which includes corrections for non-Gaussianity of both the galaxy profile and the PSF. A smaller correction is for the optical distortions in the telescope: ideally the mapping from the sky to the CCD is shape-preserving (conformal), but in reality this is not the case, resulting in a nonzero “camera shear.” In the SDSS, this is a small effect (of order 0.1 per cent) which can be identified and removed using the astrometric solution (Pier et al. 2003). Finally, a variety of systematics tests are necessary to determine that the shear responsivity \mathcal{R} has in fact been determined correctly. We refer the interested reader to Mandelbaum et al. (2005a) for the details of these corrections and tests.

One modification to the Mandelbaum et al. (2005a) pipeline is necessary for the analysis here. Mandelbaum et al. (2005a) rejected all galaxies with PHOTO’s CR or INTERP flags set, i.e. if PHOTO had to interpolate over a cosmic ray, bad CCD column, or bleed trail in order to obtain the galaxy image. These cuts are reasonable for the faint galaxies used as sources in galaxy-galaxy lensing; however, the spectroscopic galaxies typically have large area and high probability of having one of these defects present somewhere within the image. Indeed, 33 per cent of the spectroscopic galaxies are rejected by the Mandelbaum et al. (2005a) cuts, and of this subset, 88 per cent come from CR and INTERP. Moreover, signal-to-noise is not an issue for the spectroscopic galaxies, with typical detections of $\sim 100\sigma$ (versus $\sim 10\text{--}20\sigma$ for the photometric galaxies at the limit $r = 21.8$), so one does not worry about noise-related problems when doing the interpolation. We therefore replaced this cut with a cut on INTERP_CENTER, eliminating only those for which the defect was very close to the object’s center and therefore may have had a relatively larger effect on the determination of the centroid or other parameters.

4 COMPUTATION OF CORRELATION FUNCTIONS

4.1 Estimator

Our estimator for the the intrinsic alignment correlation function is a generalization of the LS (Landy & Szalay 1993) estimator for the galaxy correlation function. The LS estimator for the galaxy correlation function $\xi(r_p, \Pi)$ is

$$\hat{\xi}(r_p, \Pi) = \frac{(D - R)^2}{RR} = \frac{DD - 2DR + RR}{RR}, \quad (14)$$

where DD is the number of pairs of real (“data”) galaxies with separations r_p and Π , RR is the number of such pairs in a random catalog, and DR is the number of pairs of data and random galaxies with this separation. (DR and RR are understood to be rescaled in proportion to N_{gal} and N_{gal}^2 respectively if the number of random catalog galaxies differs from the number of data galaxies, which is usually the case.) From our perspective, the key advantage of the random catalog subtraction in Eq. (14) is that $\langle D - R \rangle = 0$. This means that if there is any additive systematic error δD in the data, we find that the bias in the correlation function is

$$\langle \delta \hat{\xi}(r_p, \Pi) \rangle = \frac{2\langle D - R \rangle \delta D + \delta D^2}{RR}; \quad (15)$$

since $\langle D - R \rangle = 0$, the bias is thus second-order in any systematic. This feature makes the LS estimator more robust than previous estimators such as $DD/RR - 1$, and is retained in most of the recent estimators for the correlation function or power spectrum.

When we compute the galaxy-intrinsic shear correlation function $\xi_{g+}(r_p, \Pi)$, we can generalize Eq. (14) to

$$\hat{\xi}_{g+}(r_p, \Pi) = \frac{S_+(D - R)}{RR} = \frac{S_+D - S_+R}{RR}, \quad (16)$$

where S_+D is the sum over all pairs with separations r_p and Π of the + component of shear:

$$S_+D = \sum_{i \neq j | r_p, \Pi} \frac{e_+(j|i)}{2\mathcal{R}}, \quad (17)$$

where $e_+(j|i)$ is the + component of the ellipticity of galaxy j measured relative to the direction to galaxy i , and \mathcal{R} is the shear responsivity. S_+R is defined by a similar equation. Averaged over a statistical ensemble, $\langle S_+ \rangle = \langle D - R \rangle = 0$, so the cancellation of systematics to first order (Eq. 15) also applies here. The subtraction of S_+R in Eq. (16) is identical with the usual random catalog subtraction procedure in galaxy-galaxy lensing studies (Sheldon et al. 2004;

Mandelbaum et al. 2005a). We emphasize that positive ξ_{g+} indicates a tendency to point towards overdensities of galaxies (i.e., radial alignment, the opposite of the convention in galaxy-galaxy lensing that positive shear indicates tangential alignment).

For the intrinsic shear-shear correlation functions $\xi_{++}(r_p, \Pi)$ and $\xi_{\times\times}(r_p, \Pi)$, we simply use the estimators

$$\hat{\xi}_{++} = \frac{S_+ S_+}{RR} \quad \text{and} \quad \hat{\xi}_{\times\times} = \frac{S_\times S_\times}{RR}, \quad (18)$$

where

$$S_+ S_+ = \sum_{i \neq j | r_p, \Pi} \frac{e_+(j|i) e_+(i|j)}{(2R)^2}, \quad (19)$$

and similarly for $S_\times S_\times$. Since $\langle S_+ \rangle = \langle S_\times \rangle = 0$, the cancellation of systematics to first order works again, i.e. the square of any spurious source of shear adds to Eq. (18) instead of the shear itself.

4.2 Implementation

We wrote two pipelines to compute the correlation functions, described below. Pipeline I is based on a tree correlation function code kindly provided by Ryan Scranton, and expanded to include quantities with spin (e.g. ellipticities), the use of bins in Π in addition to r_p , and to make the jackknife subregions have sides that are roughly equal; the jackknife method is used to obtain error estimates. Pipeline II is a “brute force” correlation function code designed to be as simple as possible; its main purpose is to provide a completely independent check on the much more sophisticated Pipeline I. Pipeline I was used for the main scientific results of this paper (except where indicated), but we have checked that these are not significantly altered by using Pipeline II instead (see the result section).

In order to find pairs of galaxies, Pipeline I uses the SDSSpix package.⁴ To avoid noise in the determination of $D - R$ in the $S_+(D - R)/RR$ estimator of the GI correlation function, we use 10 random points for each real galaxy in the catalog. The correlation functions are computed over a $120 h^{-1} \text{Mpc}$ (comoving) range along the line of sight from $\Pi = -60 h^{-1} \text{Mpc}$ to $\Pi = +60 h^{-1} \text{Mpc}$, divided into 30 bins $4 h^{-1} \text{Mpc}$ in size, and the projected correlation function is computed by “integration” (technically summation of the correlation function multiplied by $\Delta\Pi$) over Π . This calculation is done in $N_{bin} = 10$ radial bins from $0.3 < r_p < 60 h^{-1} \text{Mpc}$. (Note, however, that to avoid calculating pairs over excessively large separations, we imposed a cut such that the maximum angular separation considered is equal to that at $60 h^{-1} \text{Mpc}$ at $z = 0.05$, so the relatively small number of lower-redshift pairs do not contribute to the result at the largest values of r_p .) Covariance matrices are determined using a jackknife with 50 regions. This number was chosen to be large enough to obtain a stable covariance matrix for the fits (it must be larger than $N_{bin}^{3/2}$; see Appendix D of Hirata et al. 2004) but small enough that the size of a given jackknife region is larger than the scale on which the

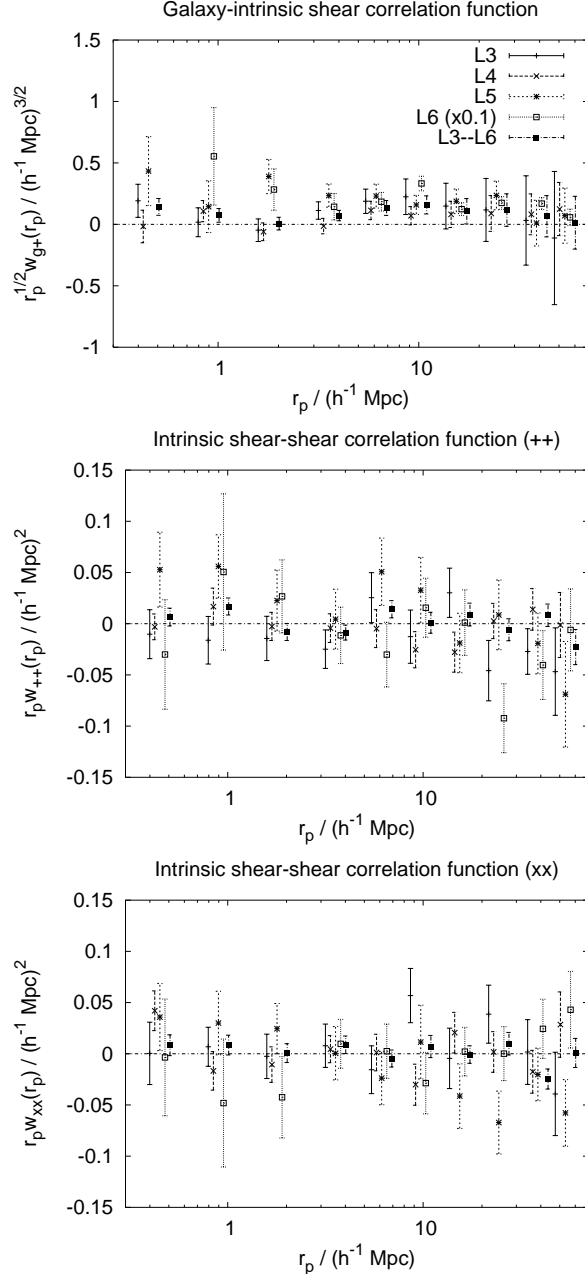


Figure 1. The correlation functions $w_{g+}(r_p)$, $w_{++}(r_p)$, and $w_{\times\times}(r_p)$ obtained from the L3, L4, L5, L6, and the full galaxy samples. Each of the 10 bins contains the same range in r_p for each of the samples, but some of the error bars have been slightly displaced horizontally for clarity (L5 has not been displaced). The L6 data have been multiplied by 0.1 so that they can fit on the same scale. All the errors are 68 per cent confidence bands, and the errorbars are highly correlated on large scales.

correlation is to be measured. Our results for the galaxy-galaxy correlation function $\xi(r_p, \Pi)$ and the projected correlation function as a function of luminosity match those in Zehavi et al. (2005), a similar analysis of SDSS data covering a smaller area of the sky.

Pipeline II is simpler in that for density-shape correlations, the $S_+ D$ estimator is used instead of $S_+ D - S_+ R$; and that there is only one bin in Π , $\Delta\Pi = 120 h^{-1} \text{Mpc}$. Because

⁴ URL: <http://lahmu.phyast.pitt.edu/~scranton/SDSSPix/>

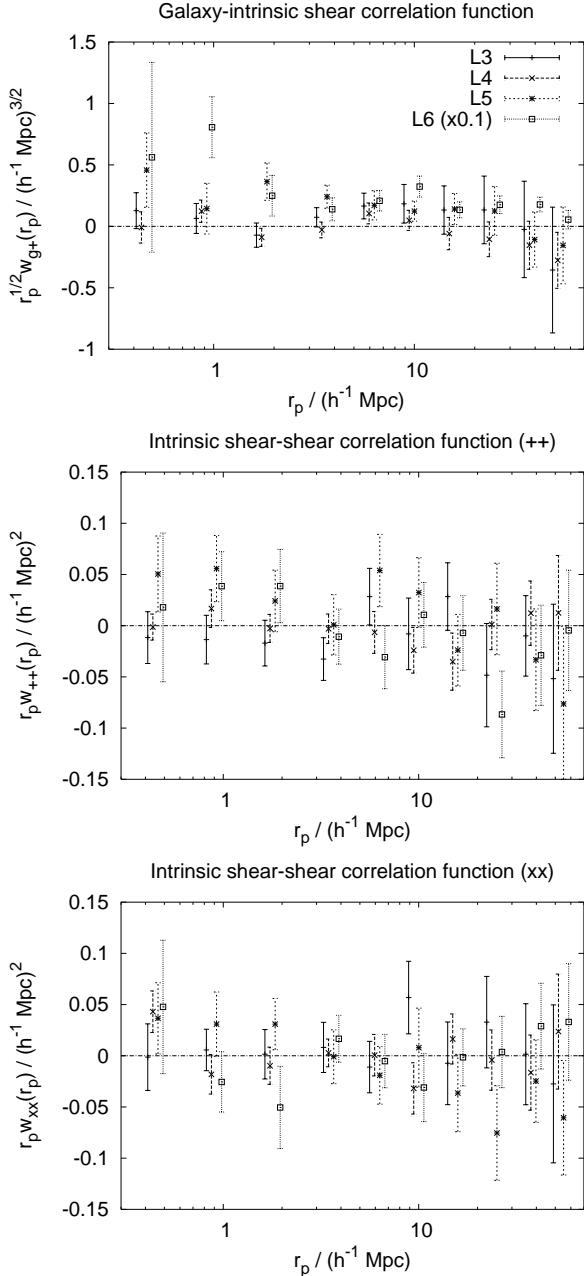


Figure 2. The correlation functions $w_{g+}(r_p)$, $w_{++}(r_p)$, and $w_{\times\times}(r_p)$ obtained from the L3–L6 galaxy samples. Same as Fig. 1 except that Pipeline II was used, and results are not shown for the full sample.

this pipeline does not use $D - R$ in any of its estimators, its calculations were completed with only one random point for every real galaxy instead of 10.

4.3 Results

The correlation functions obtained via Pipeline I are shown in Fig. 1, and via Pipeline II in Fig. 2. We note that the difference between the two results is significantly less than 1σ , indicating that these two independently written pipelines give the same result. In order to convert $w_{g\times}$ into $\Delta\gamma_{int}$ in g-g lensing for comparison against Hirata et al. (2004), it

is necessary to multiply by -1 (to account for the different ellipticity convention) and divide by $\Delta\Pi + w_{gg}(r_p)$, where $\Delta\Pi = 120h^{-1}\text{Mpc}$ and the projected correlation function can be estimated from Zehavi et al. (2005), for which the luminosity subsamples have nearly the same selection as in this work. See Appendix A of Hirata et al. (2004) for more details. Note that the results are still not quite appropriate to compare against those in Hirata et al. (2004), because the $\Delta\gamma_{int}$ so obtained from, e.g., our L6 results here would be that expected if one did g-g lensing with L6 lenses and sources only, instead of L6 lenses and all sources.

4.4 Systematics tests

4.4.1 45-degree tests

The 45-degree rotation of all sources is one of the standard tests of systematics. We compute both $w_{g\times}$ and $w_{+\times}$ in a manner analogous to the computation of the signal described in §4.2, using Pipeline I only. This computation was done for all four luminosity bins. We defer analysis of the results of these systematics tests to §5.1.1, where we show consistency of the 45-degree signals with zero.

4.4.2 Large line-of-sight separation

Another test that was performed was to compute the signal in the usual manner, but instead of integrating along the line of sight from -60 to $60 h^{-1}\text{Mpc}$, we integrate in the two ranges satisfying $30 \leq |\Pi| < 90 h^{-1}\text{Mpc}$. If any signal is found for w_{g+} , w_{++} , or $w_{\times\times}$ when computed in the usual manner, computing it over large line-of-sight separations with a null result can allow us to verify that the signal is truly of astrophysical origin rather than due to some systematic. Results described below (§5.1.1) reveal no evidence of a systematic.

4.4.3 Jackknife errors

In this section, we consider the accuracy of the jackknife errorbars, a crucial part of determining the significance of any detections and of placing constraints on non-detections. There are two competing concerns in determining the number of jackknife regions: the first is that there should be sufficient regions ($\gg N_{bin}^{3/2}$, where $N_{bin} = 10$) that the covariance matrix is not too noisy; the second is that the regions must be large enough that they are truly statistically independent. If the regions are too small compared to typical pair separations, then the lack of statistical independence could lead to underestimation of errorbars, and therefore overestimation of the significance of detections or overly tight constraints on non-detected quantities.

In order to test whether our errors are overly influenced by edge effects, we redid the comparisons of $w_{g+}(r_p)$ (using the S_+D/RR estimator), $w_{++}(r_p)$, and $w_{\times\times}(r_p)$ for L3 (which is most prone to edge effects due to its low redshift) using 25, 50, 75, 100, and 200 jackknife regions. Our expectation is that if edge effects are truly significant, then we should see the size of the errors at large r_p decrease when the number of jackknife regions is increased; our hope is that the errors will have converged for our choice of 50 regions.

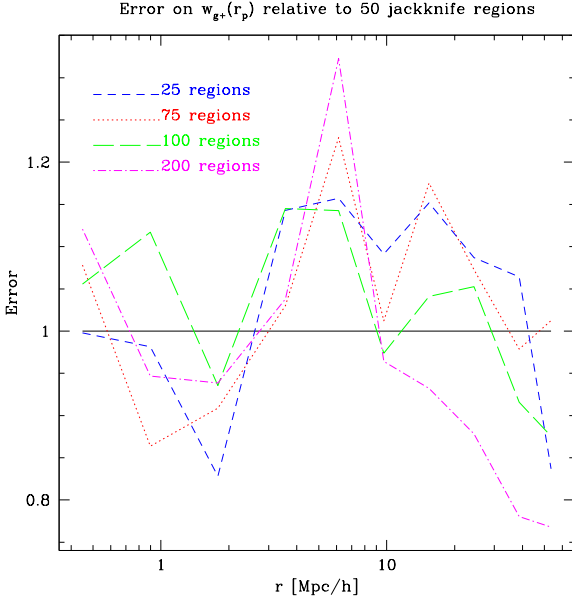


Figure 3. The size of errors of w_{g+} for L3 as a function of r_p for the density-shape correlations, relative to the size of the errors for 50 jackknife regions.

We also note that jackknife covariance matrices indicate a high correlation between radial bins on large scales, where the correlations are higher for the lower luminosity (and therefore lower redshift) bins since a given transverse separation corresponds to a larger angular separation. For example, the correlation coefficient for w_{g+} between the two outermost radial bins is 0.90, 0.95, 0.73, and 0.45 for L3, L4, L5, and L6 respectively. All analysis in the following sections includes the full covariance matrices so that the correlations are taken into account.

As shown in Fig. 3, while the errors in $w_{g+}(r_p)$ are clearly noisy at the 15 per cent level (which is unsurprising, since 50 is not that much larger than $10^{3/2} \approx 32$), there do not appear to be any significant edge effects. While the errors for the largest numbers of samples do clearly decrease on large scales relative to the errors with smaller numbers of samples, it is not apparent that there is any statistical significance to this decrease, and even if it is significant, it is not a problem for our choice of 50 jackknife regions. We have also confirmed that edge effects are not important for $w_{++}(r_p)$ and $w_{\times\times}(r_p)$. We can thus conclude that our choice of 50 jackknife regions should not cause any systematic underestimate of the errors. We address the question of whether our use of 50 jackknife regions may lead to overly noisy covariance matrices that affect our results in §5.1.1.

5 ESTIMATES OF CONTAMINATION

In this section we estimate limits on the intrinsic alignment contamination for the current and future cosmic shear surveys. Our computations here use the vanilla Λ CDM cosmology with the parameters obtained by Seljak et al. (2005b): $\Omega_b = 0.046$, $\Omega_m = 0.28$, $n_s = 0.98$, $\sigma_8 = 0.9$, and $H_0 = 71.0 \text{ km s}^{-1} \text{ Mpc}^{-1}$. Note however that the fractional error bars on our intrinsic alignment measurements are much

greater than those on the cosmological parameters, so reasonable variations in the cosmology should not substantially affect our results. We begin by fitting several intrinsic alignment models to the data (§5.1). We then consider methods of extrapolating these models from the SDSS redshift $z \sim 0.1$ to the redshifts $z \sim 1$ of interest for cosmic shear (§5.2). Then the implications for current (§5.3) and future (§5.4) cosmic shear surveys are discussed.

5.1 Model fits

We consider several models for the intrinsic alignments, which can be used to estimate the amount of contamination to weak lensing power spectra. The following types of models are considered:

1. *Power law fits:* The simplest model is a power-law fit to the intrinsic alignment correlation functions w_{g+} , w_{++} , and $w_{\times\times}$.
2. *HRH* model:* This model is designed to make our results comparable to those of Heymans et al. (2004), who presented this modified version of the HRH model originated by Heavens et al. (2000). It fits Eq. 21 below to the shape-shape correlation measurements with a free amplitude.

In any of these models, once w_{g+} , w_{++} , and $w_{\times\times}$ are determined, we can convert to $P_{g,\tilde{\gamma}^I}$, $P_{\tilde{\gamma}^I}^{EE}$, and $P_{\tilde{\gamma}^I}^{BB}$ using the Hankel transform relations (Eqs. 8–10). In the latter two cases, the power spectra are immediately useful for intrinsic alignment studies. In the former case, a conversion from g to δ must be applied. The simplest method here is the linear bias assumption, $\delta = g/b_g$, which is valid for some bias b_g on sufficiently large scales. The values of b_g (Tegmark et al. 2004; Seljak et al. 2005a) are given in Table 1, and we attempt to determine the scales on which the linear bias assumption is trustworthy using figure 9 in Tasitsiomi et al. (2004), which shows the stochasticity and bias as a function of scale determined in terms of correlation functions, i.e. $r = \xi_{gm}/\sqrt{\xi_{gg}\xi_{mm}}$ and $b^2 = \xi_{gg}/\xi_{mm}$, determined using N-body simulations. As shown there, the stochasticity is consistent with 1 for all scales larger than $400 h^{-1} \text{ kpc}$. The bottom panel indicates that the bias is approximately linear for scales larger than about $5 h^{-1} \text{ Mpc}$, but even at $1 h^{-1} \text{ Mpc}$ scale, the bias is only about 25 per cent different from its value in the linear regime.

5.1.1 Power law

The power law approach is to fit the signal to the equation:

$$w_{g+}(r_p) = A_{g+} \left(\frac{r_p}{1 h^{-1} \text{ Mpc}} \right)^{\alpha_{g+}}, \quad (20)$$

and similarly for w_{++} and $w_{\times\times}$. The fits were done by computing the χ^2 on a grid in (A_{g+}, α_{g+}) using the full jackknife covariance matrix; because this covariance matrix is noisy, the usual χ^2 analysis must be modified. Usually, it is assumed that $\Delta\chi^2$ (i.e. the difference in χ^2 between the best-fit values of the parameters and the true values) has a χ^2 distribution with a number of degrees of freedom equal to the number of parameters being fit. This is no longer the case with a noisy covariance matrix. In Appendix D of Hirata et al. (2004), we examined the distribution of the

Table 2. Best-fit parameters for power-law fits $A[r_p/(1\text{Mpc}/h)]^\alpha$ to the intrinsic alignment signal; the 95 per cent confidence intervals shown here may include no constraint on α if the amplitude is consistent with zero at this level.

Sample	function	A ($h^{-1}\text{Mpc}$)	α
L3	$w_{g+}(r_p)$	$0.082^{+0.106}_{-0.079}$	$-0.18^{+\infty}_{-\infty}$
	$w_{++}(r_p)$	$-0.018^{+0.027}_{-0.025}$	$-1.13^{+\infty}_{-\infty}$
	$w_{\times\times}(r_p)$	$0.005^{+0.030}_{-0.022}$	$-0.68^{+\infty}_{-\infty}$
L4	$w_{g+}(r_p)$	$0.020^{+0.115}_{-0.085}$	$0.013^{+\infty}_{-\infty}$
	$w_{++}(r_p)$	$(-5.7^{+1972}_{-1314}) \times 10^{-5}$	$-5.5^{+\infty}_{-\infty}$
	$w_{\times\times}(r_p)$	$(3.8^{+259}_{-3.8}) \times 10^{-4}$	$-7.1^{+5.8}_{-\infty}$
L5	$w_{g+}(r_p)$	$0.30^{+0.28}_{-0.22}$	$-0.66^{+0.54}_{-0.46}$
	$w_{++}(r_p)$	$0.031^{+0.035}_{-0.031}$	$-1.9^{+\infty}_{-\infty}$
	$w_{\times\times}(r_p)$	$0.011^{+0.030}_{-0.029}$	$-2.4^{+\infty}_{-\infty}$
L6	$w_{g+}(r_p)$	$3.8^{+3.5}_{-2.2}$	$-0.77^{+0.29}_{-0.30}$
	$w_{++}(r_p)$	$0.04^{+0.45}_{-0.48}$	$-1.8^{+\infty}_{-\infty}$
	$w_{\times\times}(r_p)$	$-0.25^{+1.05}_{-0.49}$	$-2.1^{+\infty}_{-\infty}$
All	$w_{g+}(r_p)$	$0.098^{+0.067}_{-0.069}$	$-0.59^{+0.65}_{-2.30}$
	$w_{++}(r_p)$	$(4.3^{+9.3}_{-4.3}) \times 10^{-3}$	$-2.8^{+\infty}_{-\infty}$
	$w_{\times\times}(r_p)$	$(7.2^{+13.0}_{-7.2}) \times 10^{-3}$	$-2.1^{+\infty}_{-\infty}$

jackknife or bootstrap-derived χ^2 for correlation functions computed in N bins and M regions; a similar argument allows one to determine $\Delta\chi^2$ for N bins, M regions, and K parameters. In our case, $N = 10$, $M = 50$, and $K = 2$, and the 75th, 95th, and 99th percentiles of $\Delta\chi^2$ correspond to $\Delta\chi^2 = 4.20, 9.55$, and 15.44 instead of $2.77, 5.99$, and 9.21 as derived from the standard χ^2 distribution. Thus, our confidence regions are larger than those that might be predicted naively using the standard χ^2 distribution. The resulting fits and $\Delta\chi^2$ contours (which are only strictly accurate for Gaussian error distributions) are shown in Fig. 4, and the best-fit parameters are given in Table 2 with 95 per cent confidence intervals derived using $\Delta\chi^2 = 6.17$ (the value for one variable constraints). We defer further discussion of the apparent detection of nonzero $w_{g+}(r_p)$ in L5 and L6 to section 6. The last row in Fig. 4 shows confidence regions derived from the full sample of galaxies. It is clear that the majority of our constraints come from L4.

We also performed the power-law analysis on the 45-degree rotated signals, $w_{g\times}(r_p)$ and $w_{+\times}(r_p)$, for each luminosity bin. Of the 8 signals, 7 were consistent with zero at the 68 per cent confidence level for $-4 \leq \alpha \leq 1$, and 1 was inconsistent with zero at that level but was consistent with zero at the 95 per cent confidence level. Consequently, we conclude that this test does not reveal any systematics contaminating our analysis.

Finally, we performed the power-law analysis for $w_{g+}(r_p)$ in L5 and L6 (the two bins with apparent detections) with large line-of-sight pair separations only, as described in §4.4.2. The signal computed in this manner is consistent with zero at the 68 per cent confidence level for $-4 \leq \alpha \leq 1$, which confirms that the detected signal when computed in the usual manner is indeed of astrophysical origin.

To demonstrate explicitly the goodness-of-fit of the power-law model, and the inconsistency with zero for L5,

L6, and the full sample, Table 3 includes the best-fit parameters, their χ^2 and $p(< \chi^2)$ -value, and $\Delta\chi^2 = \chi^2(A = 0) - \chi^2(\text{best fit})$ and its $p(< \Delta\chi^2)$. (Note that $p(\chi^2)$ and $p(\Delta\chi^2)$ represent the probability for a random vector to yield lower values of χ^2 or $\Delta\chi^2$ by chance, and as such is technically equal to $1 - p$, where p is the probability that the χ^2 will *exceed* the given value. Thus the $p(< \Delta\chi^2)$ for the $A = 0$ case versus for the null hypothesis tells us the confidence level at which our results exclude the null hypothesis.) Because of the noisiness of jackknife covariance matrices, the χ^2 values do not actually follow the χ^2 distribution, and the $p(< \chi^2)$ and $p(< \Delta\chi^2)$ values are therefore computed using a simulation that accounts for this fact (for more information, see Appendix D of Hirata et al. 2004). Also, to demonstrate that our results are not overly influenced by noisy covariance matrices due to the use of only 50 jackknife regions, we have repeated the analysis for 100 jackknife regions, and included the same information for that analysis in Table 3. Results for L6 use the distributions for 9 radial bins; all other bins use 10. We note that since the use of 100 jackknife regions involves different weighting of the data, the actual best-fit parameters, $\Delta\chi^2$ values, and p -values are not expected to be precisely the same as with 50 regions; however, if the fit is good, the best-fit values should be consistent with each other and the p -values for a robust detection should be small in either case.

There are a few conclusions that we can draw from Table 3. First, any changes to actual best-fit parameters due to noisiness of the jackknife covariance matrix (which would tend to affect the results with 50 jackknife regions more than with 100 jackknife regions) are much smaller than the variation allowed within the 95 per cent confidence intervals on those parameters. In both cases (50 and 100 jackknife regions), the χ^2 values for all samples except L6 are on the small side, as reflected in the $p(\Delta\chi^2)$ values tending to all be relatively small. This may reflect some overestimation of the errors and therefore underestimation of detection significance. The larger χ^2 for L6 may indicate some deviation from power-law behavior, but the actual value of χ^2 and $p(< \chi^2)$ is not sufficiently large that using this model is unreasonable. Finally, we consider the $\Delta\chi^2$ values for the special case of $A = 0$ relative to the best-fit χ^2 . As shown, the results for L3 and L4 are consistent with zero, with the $\Delta\chi^2$ not being significant. For both L5 and L6, high-significance detections were obtained whether we consider the $\Delta\chi^2$ values using 50 or 100 jackknife regions. For the full sample, the detection significance is roughly 99 per cent in both cases (slightly higher for 50 regions, slightly lower for 100 regions).

5.1.2 HRH* model

The HRH* model (Heymans et al. 2004) treats the intrinsic-intrinsic term according to:

$$\begin{aligned}
 w_{++}(r_p) &= w_{\times\times}(r_p) \\
 &= \frac{A}{8\mathcal{R}^2} \int \left[1 + \left(\frac{r}{r_0} \right)^{-\gamma} \right] \frac{1}{1 + (r/B)^2} dr_{\parallel}, \quad (21)
 \end{aligned}$$

where $r = \sqrt{r_{\parallel}^2 + r_p^2}$. Heymans et al. (2004) fit this model with the parameters $\gamma = 1.8$, $B = 1 h^{-1} \text{Mpc}$, and $r_0 = 5.25 h^{-1} \text{Mpc}$, leaving A as a free parameter. Their results

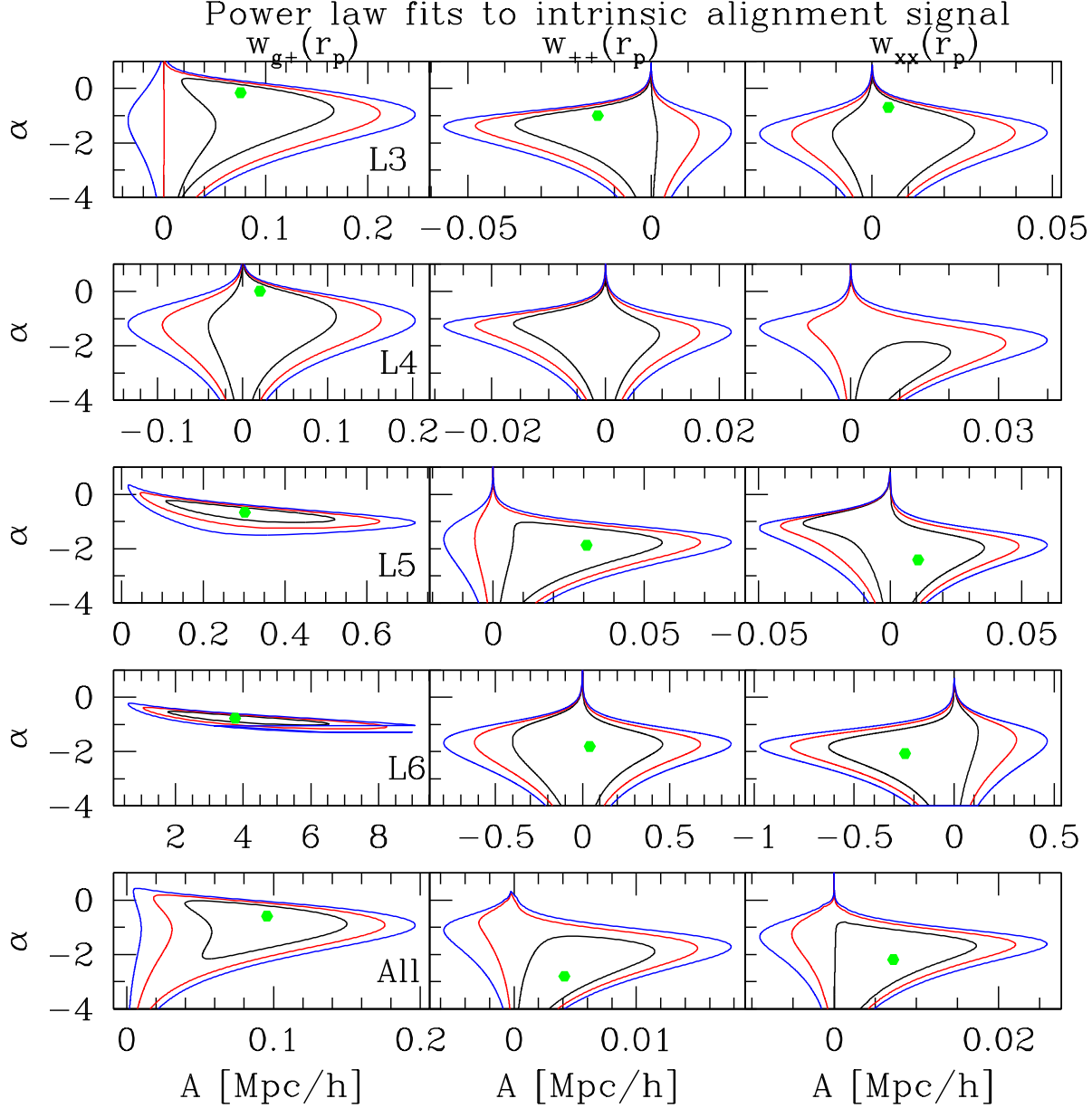


Figure 4. Power law fits to the intrinsic alignment signal from Pipeline I. From top to bottom, the rows represent the luminosity ranges L3, L4, L5, L6, and the full sample; from left to right, the columns represent the w_{g+} , w_{++} , and w_{xx} correlations respectively. The dots indicate the χ^2 minimum, and the contours represent 75, 95, and 99 per cent confidence regions. In the L6 density-shape plot, there was an insufficient number of pairs in the innermost bin to establish a reliable jackknife error estimate, so this plot is based on $N = 9$ data points.

are shown in Table 4; one can see that a detection was achieved using SuperCOSMOS. The original SuperCOSMOS intrinsic alignments analysis (Brown et al. 2002) used a median redshift of $z_{med} = 0.1$ for their sample with limiting magnitude $b_J = 20.5$, and this number was also used in the re-analysis by Heymans et al. (2004). The source of the quoted z_{med} is a parametric model from Baugh & Efstathiou (1993) using APM data, which was obtained using fits to a particular form of the redshift distribution including a parameter $z_{med}(b_J)$. It is possible that the weak dependence of z_{med} on b_J for bright galaxies assumed by the fitting for-

mula may have unduly influenced the fits, causing z_{med} to have been underestimated at intermediate magnitudes.

However, more recent data from the 2 degree Field (2dF) galaxy survey has enabled a direct measurement of the b_J band luminosity function and $k + e$ -corrections (Norberg et al. 2002), from which we find $z_{med} \sim 0.16$ for this limiting magnitude. In support of this calculation, we note that from the 2dF catalog itself (which has a limiting magnitude of $b_J = 19.45$), z_{med} for $b_J < 18.5$ is 0.082, and for $b_J < 19.45$ is 0.11. If we extrapolate the $b_J < 19.45$ number to the SuperCOSMOS flux limit using the Euclidean method, $z_{med} \sim 10^{0.2b_{J,lim}}$ (valid for $z \ll 1$)

Table 3. Best-fit parameters for power-law fits $A[r_p/(1\text{Mpc}/h)]^\alpha$ to the GI intrinsic alignment signal $w_{g+}(r_p)$ (with 95 per cent confidence intervals), the χ^2 and $p(< \chi^2)$, and $\Delta\chi^2 = \chi^2(A=0) - \chi^2(\text{best fit})$ and its $p(< \Delta\chi^2)$. These numbers are all shown for both 50 and 100 jackknife regions.

Sample	50 jackknife regions						100 jackknife regions					
	A ($h^{-1}\text{Mpc}$)	best-fit α	χ^2	$p(< \chi^2)$	($A=0$)-(best fit) $\Delta\chi^2$	$p(< \Delta\chi^2)$	A ($h^{-1}\text{Mpc}$)	best-fit α	χ^2	$p(\chi^2)$	($A=0$)-(best fit) $\Delta\chi^2$	$p(< \Delta\chi^2)$
L3	$0.082^{+0.106}_{-0.079}$	$-0.18^{+\infty}_{-\infty}$	3.9	0.09	9.6	0.95	$0.062^{+0.157}_{-0.121}$	$-0.08^{+\infty}_{-\infty}$	4.2	0.14	3.9	0.80
L4	$0.020^{+0.115}_{-0.085}$	$0.013^{+\infty}_{-\infty}$	5.7	0.23	2.1	0.51	$0.025^{+0.133}_{-0.102}$	$-0.008^{+\infty}_{-\infty}$	5.1	0.22	2.1	0.58
L5	$0.30^{+0.28}_{-0.22}$	$-0.66^{+0.54}_{-0.46}$	4.8	0.16	28.8	0.9996	$0.35^{+0.27}_{-0.26}$	$-0.73^{+0.60}_{-0.58}$	5.7	0.28	30.8	> 0.9999
L6	$3.8^{+3.5}_{-2.2}$	$-0.77^{+0.29}_{-0.30}$	12.6	0.83	48.2	> 0.9999	$3.5^{+4.5}_{-2.4}$	$-0.72^{+0.70}_{-1.0}$	11.1	0.82	54.2	> 0.9999
All	$0.098^{+0.067}_{-0.069}$	$-0.59^{+0.65}_{-2.30}$	5.9	0.25	18.8	0.996	$0.077^{+0.092}_{-0.077}$	$-0.35^{+0.65}_{-\infty}$	5.5	0.26	11.0	0.987

, we obtain $z_{med} = 0.174$. If we determine an exponential $z_{med} \sim 10^{a b_{J,lim}}$ and extrapolate that to $b_{J,lim} = 20.5$, we obtain $z_{med} = 0.144$. Both of these extrapolations merely serve as sanity checks of our result from the luminosity function calculation, and the fact that z_{med} for $b_{J,lim} = 19.45$ is already larger than 0.10 in the 2dF data further supports our assertion that the SuperCOSMOS calculations significantly underestimated z_{med} . The large underestimate of the median redshift for the SuperCOSMOS data increases the theoretical predictions for the observed signal, and hence decreases the best-fit value of A ; we therefore conclude that Heymans et al. (2004) underestimated both the value of A and its error bar. We have re-computed the theoretical predictions for the ellipticity variance at $z_{med} = 0.16$ and found the correction to be a factor of 3.0–3.4 over the range of angular scales considered by SuperCOSMOS (25–93 arc minutes). The value shown in the table has therefore had a re-scaling factor of 3.2 applied (using 3.0 or 3.4 instead changes the results by $< 0.2\sigma$). Note that the change in the redshift distribution does not affect the statistical significance of the SuperCOSMOS detection, although there are potential sources of systematic error in this data set that could lead to a spurious signal.

The constraint on A from the full SDSS sample is slightly tighter than that from SuperCOSMOS, but due to its lower central value does not provide a detection. Combining the two results is dangerous because the southern stripes of SDSS overlap with the SuperCOSMOS survey area and hence the two results are not truly independent. The results in Table 4 suggest that the SDSS and SuperCOSMOS constraints on A are mutually consistent, with any discrepancy below the 1σ level and thus not very statistically significant, particularly in light of the large systematic uncertainty due to the uncertainty in median redshift. Indeed, this comparison highlights the need for accurate redshift distributions in order to properly constrain the amplitude of intrinsic alignment correlation functions.

5.2 Redshift evolution

In order to estimate the amount of intrinsic alignment contamination in cosmic shear surveys, one must extrapolate from the SDSS redshift range $z \sim 0.05$ – 0.2 to the redshifts of the sources used in these surveys, $z \sim 0.3$ – 2 . We attempt several types of extrapolation here. Note that in each case the extrapolation becomes successively more dangerous as we go to higher redshift: our results for the lowest-redshift

Table 4. The intrinsic alignment amplitude A in Eq. (21), as determined in this paper and by Heymans et al. (2004). All results are 95 per cent confidence; the error bars from this work are determined using the jackknife confidence intervals as described in §5.1.1. The SuperCOSMOS and COMBO-17 ellipticity data are described in Bacon et al. (2000) and Brown et al. (2003), respectively. The analysis of SuperCOSMOS by Heymans et al. (2004) gave a value of $A = (0.9 \pm 0.5) \times 10^{-3}$; we have re-scaled this result by a factor of 3.2 to account for the more recent determination of the SuperCOSMOS redshift distribution. See §5.1.2 for details.

Sample	$A/10^{-3}$	Reference
SDSS L3	-1.0 ± 6.0	This work
SDSS L4	1.7 ± 4.3	This work
SDSS L5	5.8 ± 7.4	This work
SDSS L6	-43 ± 122	This work
SDSS L3–L6	1.8 ± 2.3	This work
COMBO-17	< 5.4	Heymans et al. (2004)
SuperCOSMOS	2.9 ± 1.6	Heymans et al. (2004)

surveys such as CTIO are probably very good, and any attempt to make statements at redshifts $z \approx 2$ are probably close to meaningless.

Extrapolation in redshift involves three major issues. One is that the intrinsic ellipticities of galaxies may change with time due to (for example) mergers. A second issue is that galaxies move, and thus the intrinsic alignment power spectra can change even if the orientation of each galaxy remains fixed. Finally, we have established that the intrinsic alignment signal depends on the sample of galaxies considered, and it is not clear which sample of galaxies observed at $z = 0.1$ is most similar to (or is evolved from) a particular sample of galaxies at higher redshift. Each of these issues must be addressed in the context of both the density-shape and shape-shape correlations.

In the case of the shape-shape correlation, the argument in Hirata & Seljak (2004) would suggest that in the linear regime, $w_{++}(r_p)$ and $w_{\times\times}(r_p)$ would be redshift-independent (again assuming the intrinsic ellipticities of individual galaxies do not change). Of course, most of the constraints from lensing, and most of the observational data presented here, are from nonlinear scales where the galaxy correlation function $\xi_{gg}(r_p, \Pi) \geq 1$. In the nonlinear regime, Heymans et al. (2004) argued that the correlation function

of the *unweighted* intrinsic shear γ^I would vary slowly with redshift, while the *density-weighted* correlation functions $w_{++}(r_p)$ and $w_{\times\times}(r_p)$ would increase at low z due to the growth of perturbations δ_g . In particular, if one examines the strongly nonlinear regime $\xi_{gg} \gg 1$, and assumes stable clustering with $\xi_{gg} \propto (1+z)^{-3+\gamma}$ ($\gamma \approx 1.8$ is the slope of the galaxy correlation function), then it follows that both $w_{++}(r_p)$ and $w_{\times\times}(r_p)$ should scale as $(1+z)^{-3+\gamma}$.

However, if one takes seriously the concept of stable clustering, then the unweighted intrinsic shear correlation function, $\xi_{\gamma^I\gamma^I}$, should be constant when measured in physical rather than comoving separation. In this case, the correlation functions of $\tilde{\gamma}^I$ at redshift z are

$$\xi_{++}(r_p, r_{\parallel}; z) = (1+z)^{-3} \xi_{++} \left(\frac{r_p}{1+z}, \frac{r_{\parallel}}{1+z}; 0 \right). \quad (22)$$

Integration over r_{\parallel} then gives

$$w_{++}(r_p; z) = (1+z)^{-2} w_{++} \left(\frac{r_p}{1+z}; 0 \right), \quad (23)$$

and similarly for $w_{\times\times}(r_p)$.

In the case of the density-shape correlation, the simplest prescription was provided by Hirata & Seljak (2004), who argued that if the intrinsic ellipticities of individual galaxies did not change, then on linear scales $w_{\delta+}(r_p)$ would scale as the growth factor. On the other hand, on nonlinear scales, stable clustering would suggest

$$w_{\delta+}(r_p; z) = (1+z)^{-2} w_{\delta+} \left(\frac{r_p}{1+z}; 0 \right), \quad (24)$$

in analogy to Eq. (23). The analyses below consider both the linear evolution and the stable clustering methods for extrapolating the signal to high redshift. We do not consider other methods of extrapolation since these would likely be much more complicated and it is not clear that they would have higher fidelity.

5.3 Current surveys

In the past several years, a number of cosmic shear surveys have reported results for σ_8 , which is the cosmological parameter most readily accessible to cosmic shear. It is apparent that there is some disagreement between the determinations (see, e.g., Table 1 of Heymans et al. 2005). While the differences may arise due to shear calibration biases of up to 15 per cent between the PSF correction methods used (see, e.g., Hirata & Seljak 2003a and Heymans et al. 2005) or uncertainties in z_m , there is also the possibility that the samples used for each of these studies were contaminated by intrinsic alignments in very different ways. Unfortunately, the determination of how our results apply to these samples is highly nontrivial. We have selected our galaxies in the r band at $z \sim 0.1$, but the cosmic shear selection at $z \sim 0.6$ – 1.0 is usually in the observed-frame red/far-red bands (similar to SDSS r or i), which is frequently in the rest-frame ultraviolet. This makes it very difficult to determine whether the samples in those tables correspond to the lower-contamination $L < L_*$ samples, or the higher-contamination $L > L_*$ samples.

In principle, one possible method of determining the correspondence between samples would be to use a simple

one-parameter family of templates from the stellar population synthesis code described in Bruzual & Charlot (2003) with exponential star-formation rates. Even this simple model can be shown to accurately reproduce the colors of SDSS main spectroscopic sample galaxies over for $0 < z < 0.25$. One could then find the regions in the color-color and color-magnitude diagrams corresponding to each of the luminosity bins, use the models to evolve them in redshift, and see what they looked like at $z \sim 0.6$ – 1.0 . However, such a procedure entails enough systematic uncertainty that it is unclear whether the results would be trustworthy. Hence, we defer a detailed discussion of how the detected GI alignments contaminate the results of current surveys to future work.

It is interesting to note that on small scales the GI effect on the observed angular shear correlation function may have been detected in the Red-sequence Cluster Survey (RCS). Hoekstra et al. (2004) observed an anticorrelation between the shapes of bright ($19 < R_C < 21$) and faint ($21.5 < R_C < 24$) galaxies. This anticorrelation is not consistent with either cosmic shear or estimates of the systematic errors in RCS, and Hoekstra et al. (2004) attributed it to the alignment of the bright galaxies with the ellipticities of their dark matter haloes (which lens the more distant, faint galaxies).⁵ The halo ellipticity will tend to lead to a stronger lensing signal along the lens major axis, i.e. stronger source tangential ellipticity along this axis, and therefore an anticorrelation of lens and source ellipticities. This halo ellipticity effect is a special case of the density-intrinsic shape correlation, although the physical explanation in terms of alignment of galaxy light with halo mass distribution suggests it would be limited to scales below the virial radius of the halos. On larger scales, such an anticorrelation can be interpreted as ellipticity of local large-scale structure rather than of individual halos. Of course, the galaxy samples in Hoekstra et al. (2004) were selected by putting most of the “lenses” at lower redshift than the “sources,” which Hirata & Seljak (2004) argued maximizes the GI effect. Nevertheless, precisely this type of separation of source screens has been proposed for cosmic shear tomography studies. The apparent detection of halo ellipticity also suggests that in some cases, the GI effect can exceed 100 per cent of the GG effect and result in negative shear correlation functions. Of course, such regimes must be avoided for cosmic shear studies.

5.4 Future surveys

The GI contamination estimated using the power-law fits is shown in Fig. 5 and the II contamination in Fig. 6 for a cosmic shear survey with a median redshift of $z_{med} = 1.0$. The full sample (L3–L6) GI results should be treated with caution because they are obtained by averaging the various galaxy samples whose GI contamination amplitudes are

⁵ Mandelbaum et al. (2005b) did not find such a correlation in the SDSS, but the samples of galaxies used were very different, and both Mandelbaum et al. (2005b) and this work suggest that these correlations are strongly dependent on the sample of galaxies considered.

not consistent with each other. The average is thus appropriate to the SDSS spectroscopic sample, or other samples at the same redshift range with the same selection criteria, but may not be a good guide otherwise. In particular, when considering GI contamination for a future survey, one must determine which of the luminosity subsamples is most similar to the sources to be used in that survey.

Fig. 7 shows the estimated fractional GI contamination for a survey with $z_{med} = 0.6$ (determined using linear evolution, though both methods give nearly identical results for these low redshifts) only for those samples that had a statistically significant determination of signal. A comparison between Figs. 5 and 7 shows that the contamination is more severe at lower redshifts, as expected.

We note that, as discussed in §5.1, these estimates of contamination are not reliable on small scales due to the breakdown of the linear bias assumption. At $< 1 h^{-1}\text{Mpc}$, or $L > \sim 1000$ at $z_{med} = 1$, we may be overestimating the bias by approximately 30 per cent, and consequently underestimating the contamination by that amount.

5.5 Cosmic shear tomography

Thus far we have only discussed the effects of intrinsic alignments on cosmic shear autocorrelation studies. In this section, we also consider the effects on cosmic shear tomography, the cross-correlation of pairs widely separated in redshift, either via down-weighting pairs close in photometric redshift, or by explicitly separating into multiple samples based on photometric redshift or apparent magnitude such that the samples lie in distinct regions in redshift. In principle, while the cross-correlation should still give a GG signal due to lensing by structures between the observer and the lower-redshift source sample, any intrinsic alignment II contamination will be highly suppressed. However, as pointed out in Hirata & Seljak (2004), the GI contamination may still be significant when selecting pairs separated in redshift space, because the galaxy at lower redshift can be aligned with the same tidal field that lenses the higher-redshift galaxy of the pair. In light of our robust detection of the GI contamination using pairs at the same redshift, more investigation into the effect of this contamination on cosmic shear tomography is warranted; this investigation is beyond the scope of this paper. Some of these issues have been investigated by King (2005).

6 INTRINSIC ALIGNMENTS AND BCGS

An early study of alignments of cluster galaxy ellipticities with the cluster major axis, Binggeli (1982), found a tendency for brightest cluster galaxies (BCGs) to align with the cluster ellipticity using 44 Abell clusters with $z < 0.1$. Later studies confirmed this ‘‘Binggeli effect,’’ Fuller et al. (1999) with poor clusters, West & Blakeslee (2000) in 3 dimensions for the Virgo cluster, and Kim et al. (2002) using ~ 300 clusters in SDSS data over a large range in redshift, $0.04 < z < 0.5$. This effect has been explained in terms of anisotropic infall along filaments (West 1989), an explanation that is supported by numerous N -body simulations (e.g. Dubinsky 1998). [The related ‘‘Holmberg effect’’ (Holmberg 1969), the correlation of

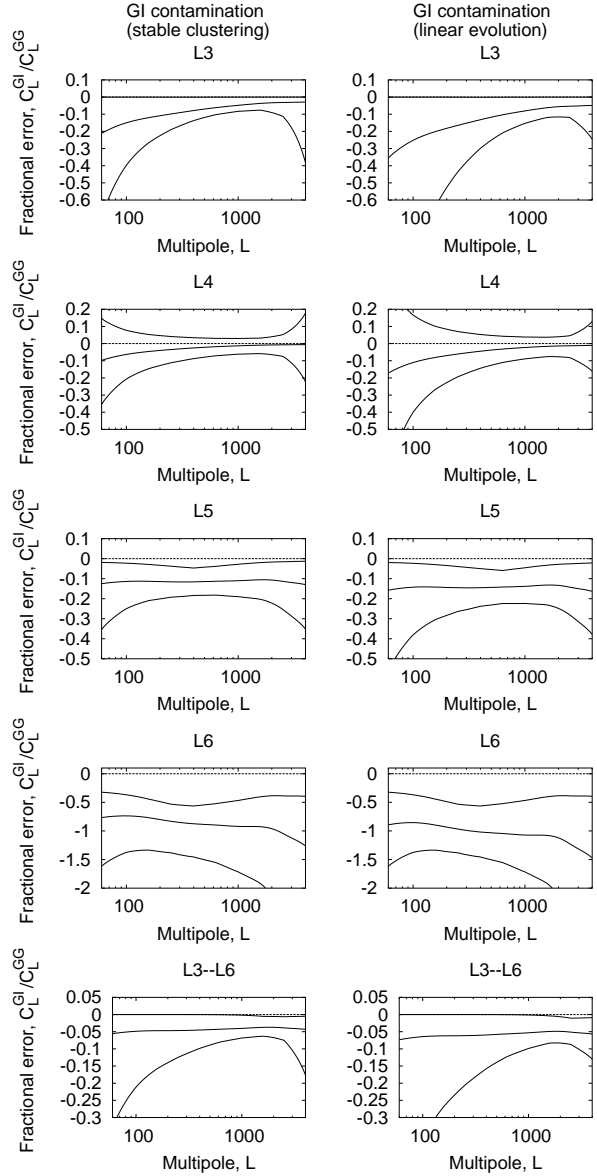


Figure 5. The allowed range of GI contamination for each luminosity subsample. The power-law fits are used, with the left column showing the results for the stable clustering assumption and the right column showing the results for linear evolution as argued by Hirata & Seljak (2004). The bottom and top curves show the 95 per cent confidence region assuming a power law intrinsic alignment model with index $-3 < \alpha_{g+} < +1$. The center curve shows the contamination predicted by the best-fit parameters in Table 2. The median source redshift assumed is $z_{med} = 1.0$. [The constraints on α_{g+} are imposed because for $\alpha_{g+} \geq +1$ or $\alpha_{g+} \leq -4$, the Hankel transform defining $P_{\delta, \bar{\gamma}_I}(k)$ becomes ill-defined. A cutoff value greater than -4 was chosen because otherwise the correlations at very small scales dominates the power spectrum. Note that in the cases of L5 and L6 where we have a detection, α_{g+} is constrained to lie within the range given here at > 99 per cent confidence.]

satellite positions with the major axis of the primary (not in clusters), has also been studied fairly extensively observationally (Hawley & Peebles 1975; Valtonen et al. 1978; MacGillivray et al. 1982; Zaritsky et al. 1997; Sales & Lambas 2004; Brainerd 2005) and with simulations (Navarro et al. 2004; Azzaro et al. 2005; Kang et al. 2005; Libeskind et al. 2005; Zentner et al. 2005), and is another possible explanation, though unlike for clusters the results – magnitude and even sign of the effect – have been conflicting.] This effect may be used to explain the detection of nonzero $w_{g+}(r_p)$ in L5 and L6: if some of these bright galaxies are BCGs of clusters, then we expect to find an overdensity of galaxies along their major axis, leading to positive w_{g+} . In support of this hypothesis, we note that the majority of these bright galaxies are red, and many pass the color cuts to be included in the SDSS spectroscopic LRG sample; it is well known that BCGs tend to be red galaxies.

Naturally, BCG alignments can only explain a detection on small ($< \sim 2 h^{-1}\text{Mpc}$) scales. However, when combined with the result (Hopkins et al. 2005) that clusters themselves are aligned with each other for separations up to $100 h^{-1}\text{Mpc}$, we can also explain the larger scale alignments, since it means that a BCG of a given cluster also tends to point preferentially towards overdensities of galaxies on larger scales and not just within its own cluster. We also note the result shown there (from N -body simulations) that the alignment increases with increasing redshift, indicating that if our explanation of the effect is correct, then it may be worse for higher-redshift surveys than what has been detected here.

If indeed the major source of density-shape correlation is BCG alignment, it may be advantageous for cosmic shear surveys to reject BCGs, particularly in the lower-redshift bins where their intrinsic alignments can contaminate the cross-correlation tomography signal. A variety of algorithms exist to identify clusters and their BCGs (e.g. Gladders & Yee 2000; Goto et al. 2002; Bahcall et al. 2003), and it is beyond the scope of this paper to examine how much the density-shape correlation can be suppressed by rejecting BCGs selected by each of these methods.

Pereira & Kuhn (2005) use X-ray selected clusters with SDSS photometric and spectroscopic imaging data to find a tendency for radial alignment of cluster galaxies, not limited to BCGs. To explain their findings, they propose a parametric resonance phenomenon that causes a tendency for many cluster galaxies to exhibit radial alignment relative to the cluster center. Their results suggest that removing BCGs from the sample may not be sufficient to eliminate GI contamination. Further investigation of our results, including a search for intrinsic alignments that distinguishes between satellites in clusters and the BCGs themselves, is necessary to understand the degree to which the effect they observe is important for cosmic shear surveys.

We also note that the effect seen here is related to the effect seen by correlating positions of a fainter set of galaxies with the position angles of lens galaxies in Mandelbaum et al. (2005b). There, as shown in Figure 6 and the accompanying text, a statistically significant tendency for the fainter galaxies to be positioned along the major axis of the central galaxy was found for L5 and L6.

7 CONCLUSIONS

We have used the SDSS main spectroscopic sample to search for II and GI correlations by computing projected correlation functions $w_{g+}(r_p)$, $w_{++}(r_p)$, and $w_{\times\times}(r_p)$ over the range of pair separations $0.3 < r_p < 60 h^{-1}\text{Mpc}$. We have two main results coming out of these calculations.

The first result is a constraint on the II correlation, expressed in terms of several models in §5.1 and in terms of projected contamination for higher-redshift surveys in §5.4. As shown, we have no detection of II correlations either in luminosity bins or using the full sample. The limits rule out a significant contamination of shear signal by II, although contamination at the 10 per cent level for lensing surveys at $z_s \sim 1$ is still a possibility. Thus, the II correlation may still be a concern for future cosmic shear surveys with expected statistical errors below the 1 per cent level, though it can be minimized by cross-correlating source galaxies in different redshift slices.

The second result is a detection of GI correlations for $L > L_*$ galaxies (L5 and L6), as well as for the overall sample, with nonzero amplitude of the correlation function $w_{g+}(r_p)$ for the power-law subscript $-4 \leq \alpha \leq 1$, at the > 99 per cent confidence level. We have no detection of GI correlations for $L \leq L_*$ galaxies (L3 and L4), and have placed constraints on them for the first time. The agreement of our results from two independent pipelines to calculate the correlation functions confirms the robustness of our findings. As for the II correlations, we have used several models of extrapolating these GI results to higher-redshift cosmic shear autocorrelation power spectra in §5.4 to predict GI contamination at $z_s = 1$ and $L = 100 - 1000$ of 5–25 per cent (L5), 50–150 per cent (L6), or 0–15 per cent (full sample). These GI correlations are positive in sign, which is the opposite of the GG lensing induced signal, so the interference is destructive (Hirata & Seljak 2004). As a result the amplitude of fluctuations is systematically underestimated in current surveys where this effect has been ignored. The estimated error in the linear amplitude σ_8 from this effect is uncertain, but estimates presented here suggest current surveys underestimate it by 0–20 per cent for $z_s \sim 1$ and possibly up to 30 per cent for shallower surveys with $z_s \sim 0.5$.

These results leave open a number of questions for future work. First, is there some way to minimize the contamination due to the GI correlations, which cannot be eliminated by the scheme proposed for eliminating II correlations via cross-correlation of sources at different redshifts? We have proposed BCG alignments with cluster ellipticities as a possible explanation for the correlation, so eliminating BCGs from the sample used for computing cosmic shear should be investigated as a means of reducing this alignment, though as suggested by Pereira & Kuhn (2005), this step alone may not be sufficient. Second, what are the implications of the GI detection for current cosmic shear studies, and could they explain the conflicting values of σ_8 (which do have other possible explanations, such as shear calibration bias or uncertainty in redshift distributions)? In order to investigate this question thoroughly, it will be necessary to determine the correspondence between the samples used for this work and for the current cosmic shear studies. Finally, it is clear that a systematic error at a 10 per cent level cannot be tolerated in future surveys such as LSST, PanStarrs

or JDEM, which require a sub-percent precision to achieve the stated goals. More detailed implications for future work, including cosmic shear tomography, which is susceptible to contamination from the GI detection, will be addressed in a following work, Ishak et al. (2005).

In summary, our detection of the GI contamination of the cosmic shear power spectrum should serve as a useful starting point for further investigation into this effect, which is one of the main theoretical uncertainties in understanding current cosmic shear analyses, and may also lead to methods that can help reduce this contamination to the lowest level possible when interpreting data from future surveys.

ACKNOWLEDGMENTS

RM is supported by an NSF Graduate Research Fellowship. CH is supported in part by NSF PHY-0503584 and by a grant-in-aid from the W. M. Keck Foundation. MI acknowledges the support of the Natural Sciences and Engineering Research Council of Canada (NSERC) and NASA Theory Award NNG04GK55G.

We wish to thank Ryan Scranton for the use of his correlation function code. We thank David Spergel for pointing out some relevant references, Catherine Heymans for useful discussion of results, and Michael Brown for clarification regarding the SuperCOSMOS dataset. Finally, we thank the referee for useful suggestions that help strengthen the conclusions of the paper.

Funding for the creation and distribution of the SDSS Archive has been provided by the Alfred P. Sloan Foundation, the Participating Institutions, the National Aeronautics and Space Administration, the National Science Foundation, the U.S. Department of Energy, the Japanese Monbukagakusho, and the Max Planck Society. The SDSS Web site is <http://www.sdss.org/>.

The SDSS is managed by the Astrophysical Research Consortium (ARC) for the Participating Institutions. The Participating Institutions are The University of Chicago, Fermilab, the Institute for Advanced Study, the Japan Participation Group, The Johns Hopkins University, the Korean Scientist Group, Los Alamos National Laboratory, the Max-Planck-Institute for Astronomy (MPIA), the Max-Planck-Institute for Astrophysics (MPA), New Mexico State University, University of Pittsburgh, University of Portsmouth, Princeton University, the United States Naval Observatory, and the University of Washington.

REFERENCES

- Abazajian K. et al., 2003, *AJ*, 126, 2081
 Abazajian K., Dodelson S., 2003, *PRL*, 91, 041301
 Abazajian K. et al., 2004, *AJ*, 128, 502
 Abazajian K. et al., 2005, *AJ*, 129, 1755
 Adelman-McCarthy J. et al., 2005, *ApJS* submitted (astro-ph/0507711).
 Azzaro M., Zentner A. R., Prada F., Klypin A., 2005, preprint (astro-ph/0506547)
 Bacon D. J., Refregier A. R., Ellis R. S., 2000, *MNRAS*, 318, 625
 Bacon D. J., Refregier A., Clowe D., Ellis R. S., 2001, *MNRAS*, 325, 1065
 Bahcall N. A., et al., 2003, *ApJS*, 148, 243
 Bartelmann M., Schneider P., 2001, *Phys. Rep.*, 340, 291
 Baugh C. M., Efstathiou, G., 1993, *MNRAS*, 265, 145
 Benabed K., Van Waerbeke L., 2004, *PRD*, 70, 123515
 Bernstein G. M., Jain B., 2004, *ApJ*, 600, 17
 Bernstein G. M., Jarvis M., 2002, *AJ*, 123, 583
 Bernstein G. M., Norberg P., 2002, *AJ*, 124, 733
 Binggeli B., 1982, *A&A*, 107, 338
 Blanton M. R., Lin H., Lupton R. H., Maley F. M., Young N., Zehavi I., Loveday J., 2003a, *AJ*, 125, 2276
 Blanton M. R. et al., 2003b, *AJ*, 125, 2348
 Blanton M. R., et al. 2003c, *ApJ*, 592, 819
 Blanton M. R. et al., 2005, *AJ*, 129, 2562
 Brainerd T. G., Blandford R. D., Smail I., 1996, *ApJ*, 466, 623
 Brainerd T. G., 2005, *ApJL*, 628, L101
 Brown M. L., Taylor A. N., Hambly N. C., Dye S., 2002, *MNRAS*, 333, 501
 Brown M. L., Taylor A. N., Bacon D. J., Gray M. E., Dye S., Meisenheimer K., Wolf C., 2003, *MNRAS*, 341, 100
 Bruzual G., Charlot S., 2003, *MNRAS*, 344, 1000
 Budavári T., Szalay A. S., Connolly A. J., Csabai I., Dickinson M., 2000, *AJ*, 120, 1588
 Catelan P., Kamionkowski M., Blandford R. D., 2001, *MNRAS*, 320, L7
 Colless M., Dalton G., Maddox S., Sutherland W., Norberg P., Cole S. et al., 2001, *MNRAS*, 328, 1039
 Cooray A., Hu W., 2002, *ApJ*, 574, 19
 Cooray A., Kamionkowski M., Caldwell R., 2005, *PRD*, 71, 123527
 Crittenden R. G., Natarajan P., Pen U., Theuns T., 2001, *ApJ*, 559, 552
 Croft R. A. C., Metzler C. A., 2000, *ApJ*, 545, 561
 Csabai I., Connolly A. J., Szalay A. S., Budavári T., 2000, *AJ*, 119, 69
 Csabai I. et al., 2003, *AJ*, 125, 580
 Dubinski J., 1998, *ApJ*, 502, 141
 Eisenstein D. J. et al., 2001, *AJ*, 122, 2267
 Erben T., Van Waerbeke L., Bertin E., Mellier Y., Schneider P., 2001, *A&A*, 366, 717
 Finkbeiner D. et al., 2004, *AJ*, 128, 2577
 Fischer P., Tyson J. A., 1997, *AJ*, 114, 14
 Fischer P. et al., 2000, *AJ*, 120, 1198
 Fukugita M., Ichikawa T., Gunn J. E., Doi M., Shimasaku K., Schneider D. P., 1996, *AJ*, 111, 1748
 Fuller T. M., West M. J., Bridges T. J., 1999, *ApJ*, 519, 22
 Gladders M. D., Yee H. K. C., 2000, *AJ*, 120, 2148
 Goto T., et al., 2002, *AJ*, 123, 1807
 Gunn J. E., Carr M., Rockosi C., Sekiguchi M., et al., 1998, *AJ*, 116, 3040
 Gunn J. E. et al., 2005, *AJ*, submitted
 Guzik J., Seljak U., 2002, *MNRAS*, 335, 311
 Heavens A., Refregier A., Heymans C., 2000, *MNRAS*, 319, 649
 Heymans C., Heavens A., 2003, *MNRAS*, 339, 711
 Heymans C., Brown M., Heavens A., Meisenheimer K., Taylor A., Wolf C., 2004, *MNRAS*, 347, 895
 Heymans C. et al., 2005, preprint (astro-ph/0506112)
 Hirata C. M., Seljak U., 2003a, *MNRAS*, 343, 459
 Hirata C. M., Seljak U., 2003b, *PRD*, 68, 083002

- Hirata C. M., Seljak U., 2004, PRD, 70, 063526
Hirata C. M. et al., 2004, MNRAS, 353, 529
Hoekstra H., 2004, MNRAS, 347, 1337
Hoekstra H., Franx M., Kuijken K., Squires G., 1998, ApJ, 504, 636
Hoekstra H., Franx M., Kuijken K., 2000, ApJ, 532, 88
Hoekstra H. et al., 2001, ApJL, 548, L5
Hoekstra H., Yee H. K. C., Gladders M. D., Barrientos L. F., Hall P. B., Infante L., 2002, ApJ, 572, 55
Hoekstra H., Franx M., Kuijken K., Carlberg R. G., Yee H. K. C., 2003, MNRAS, 340, 609
Hoekstra H., Yee H. K. C., Gladders M. D., 2004, ApJ, 606, 67
Hawley D. L., Peebles P. J. E., 1975, AJ, 80, 477
Hogg D. W., Finkbeiner D. P., Schlegel D. J., Gunn J. E., 2001, AJ, 122, 2129
Holmberg E., 1969, Arxiv Astron., 5, 305
Hopkins P. F., Bahcall N. A., Bode P., 2005, ApJ, 618, 1
Hu W., 2002, PRD, 65, 023003
Hudson M. J., Gwyn S. D. J., Dahle H., Kaiser N., 1998, ApJ, 503, 531
Huterer D., 2002, PRD, 65, 063001
Hui L., Zhang J., 2002, preprint (astro-ph/0205212)
Huterer D., Takada M., Bernstein G., Jain B., 2005, preprint (astro-ph/0506030)
Ishak M., 2005, MNRAS, 363, 469
Ishak M., Hirata C., Mandelbaum R., 2005, in preparation
Ishak M., Hirata C., McDonald P., Seljak U., 2004, PRD, 69, 083514
Ishak M., Hirata C., 2005, PRD, 71, 023002
Ivezić Ž. et al., 2004, Astron. Nachr., 325, 583
Jarvis M., Bernstein G. M., Fischer P., Smith D., Jain B., Tyson J. A., Wittman D., 2003, AJ, 125, 1014
Jing Y. P., 2002, MNRAS, 335, L89
Kaiser N., 2000, ApJ, 537, 555
Kaiser N., Squires G., Broadhurst T., 1995, ApJ, 449, 460
Kang X., Mao S., Gao L., Jing Y. P., 2005, A&A, 437, 383
Kim R. S. J., Annis J., Strauss M. A., Lupton R. H., 2002, in ASP Conf. Ser. 268: Tracing Cosmic Evolution with Galaxy Clusters, p. 395
King L., Schneider P., 2002, A&A, 396, 411
King L., 2005, A&A, 441, 47
Landy S., Szalay A., 1993, ApJ, 412, 64
Lee J., Pen U., 2000, ApJL, 532, L5
Lee J., Pen U., 2001, ApJ, 555, 106
Lee J., Pen U., 2002, ApJL, 567, L111
Libeskind N. I., Frenk C. S., Cole S., Helly J. C., Jenkins A., Navarro J. F., Power C., 2005, MNRAS, 363, 146
Luppino G. A., Kaiser N., 1997, ApJ, 475, 20
Lupton R., Gunn J. E., Ivezić Ž., Knapp G. R., Kent S., Yasuda N., 2001, in ASP Conf. Ser. 238, *Astronomical Data Analysis Software and Systems X*, ed. Harnden F. R. Jr., Primi F. A., Payne H. E. (San Francisco: Astr. Soc. Pac.), p. 269
Ma Z., Hu W., Huterer D., 2005, preprint (astro-ph/0506614)
MacGillivray H. T., Dodd R. J., McNally B. V., Corwin H. G., 1982, MNRAS, 198, 605
Maddox S. J., Efstathiou G., Sutherland W. J., Loveday J., 1990, MNRAS, 243, 692
Mandelbaum R. et al., 2005a, MNRAS, 361, 1287
Mandelbaum R., Hirata C. M., Broderick T., Seljak U., Brinkmann J., 2005b, preprint (astro-ph/0507108)
McKay T. A. et al., 2001, preprint (astro-ph/0108013)
Mellier Y., 1999, ARA&A, 37, 127
Miralda-Escudé J., 1991, ApJ, 380, 1
Navarro J., Abadi M., Steinmetz M., 2004, ApJL, 613, L41
Norberg P. et al., 2002, MNRAS, 336, 907
Padmanabhan N. et al., 2004, New Astron., 9, 329
Pen U., Lee J., Seljak U., 2000, ApJL, 543, L107
Pereira M. J., Kuhn J. R., 2005, ApJL, 627, L21
Pier J. R., Munn J. A., Hindsley R. B., Hennessy G. S., Kent S. M., Lupton R. H., Ivezić Ž., 2003, AJ, 125, 1559
Rawlings S., Abdalla F. B., Bridle S. L., Blake C. A., Baugh C. M., Greenhill L. J., van der Hulst J. M., 2004, New Astron. Rev., 48, 1013
Refregier A., 2003a, ARA&A, 41, 645
Refregier A., 2003b, MNRAS, 338, 35
Refregier A., Bacon D., 2003, MNRAS, 338, 48
Rhodes J., Refregier A., Groth E. J., 2001, ApJ, 552, L85
Richards G. et al., 2002, AJ, 123, 2945
Sales L., Lambas D. G., 2004, MNRAS, 348, 1236
Schlegel D. J., Finkbeiner D. P., Davis M., 1998, ApJ, 500, 525
Schneider P., van Waerbeke L., Mellier Y., 2002, A&A, 389, 729
Seljak U. et al., 2005a, PRD, 71, 043511
Seljak U. et al., 2005b, PRD, 71, 103515
Sheldon E. S. et al., 2001, ApJ, 554, 881
Sheldon E. S. et al., 2004, AJ, 127, 2544
Smith J. A. et al., 2002, AJ, 123, 2121
Song Y. S., Knox L., 2005, PRD, 71, 024026
Spergel D. N. et al., 2003, ApJS, 148, 175
Stoughton C., Lupton R. H., et al., 2002, AJ, 123, 485
Strauss M. A., Weinberg D. H., Lupton R. H., Narayanan V. K., et al., 2002, AJ, 124, 1810
Tasitsiomi A., Kravtsov A. V., Wechsler R. H., Primack J. R., 2004, ApJ, 614, 533
Tegmark M. et al., 2004, ApJ, 606, 702
Tereno I., Dore D., Van Waerbeke L., Mellier Y., 2005, A&A, 429, 383
Tucker D. et al., 2005, AJ, submitted
Upadhye A., Ishak M., Steinhardt P., 2005, PRD, 72, 063501
Vale C., Hoekstra H., White M., 2004, ApJL, 613, L1
Valtonen M. J., Teerikorpi P., Argue A. N., 1978, AJ, 83, 135
Van den Bosch F. C., Abel T., Croft R. A. C., Hernquist L., White S. D. M., 2002, ApJ, 576, 21
Van Waerbeke L. et al., 2000, A&A, 358, 30
Van Waerbeke L., Mellier Y., Pelló R., Pen U.-L., McCracken H. J., Jain B., 2002, A&A, 393, 369
Van Waerbeke L., Mellier Y., Hoekstra H., 2005, A&A, 429, 75
West M. J., 1989, ApJ, 347, 610
West M. J., Blakeslee J. P., 2000, ApJL, 543, L27
White M., 2004, Astropart. Phys., 22, 211
White M., Vale C., 2004, Astropart. Phys., 22, 19
York D. G., et al., 2000, AJ, 120, 1579
Zaritsky D., Smith R., Frenk C. S., White D. M., 1997, ApJL, 478, L53
Zentner A. R., Kravtsov A. V., Gnedin O. Y., Klypin A. A., 2005, ApJ, 629, 219

Zehavi I., et al., 2005, ApJ, 630, 1

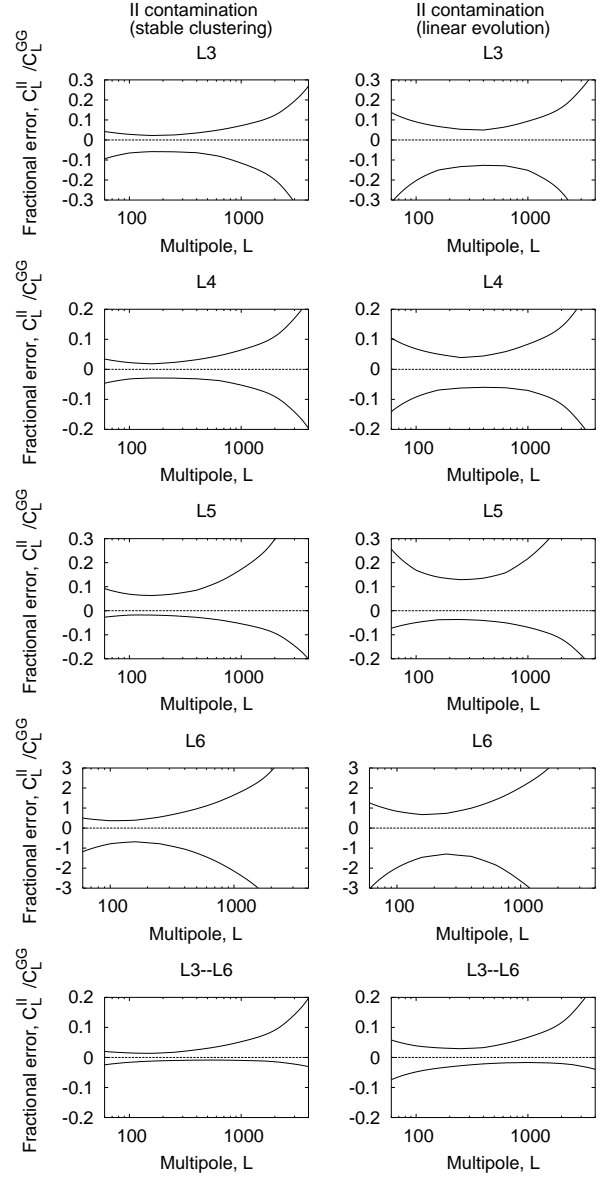


Figure 6. The allowed range of II contamination for each luminosity subsample. The power-law fits are used, with the left column showing the results for the stable clustering assumption and the right column showing the results for linear evolution as argued by Hirata & Seljak (2004). The bottom and top curves show the 95 per cent confidence region assuming a power law intrinsic alignment model with index $-1.5 < \alpha < 0$. The median source redshift assumed is $z_{med} = 1.0$. [The constraints on α are imposed because for $\alpha_{++} \geq +0$ or $\alpha_{++} \leq -2$, the Hankel transform defining $P_{\delta, \tilde{\gamma}I}(k)$ becomes ill-defined. A cutoff value greater than -2 was chosen because otherwise the correlations at very small scales dominates the power spectrum. We do not detect II in any of these cases, so the actual power law slope cannot be determined from the data.]

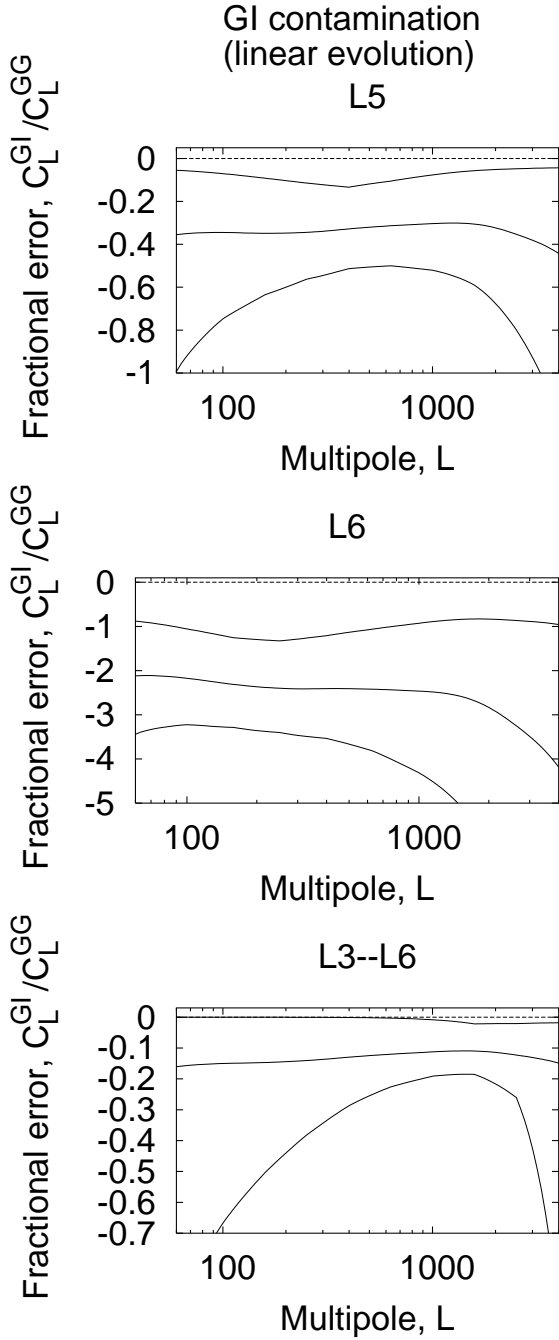


Figure 7. The allowed range of GI contamination for L5, L6, and the full sample determined using the power-law fits and linear evolution for $z_{med} = 0.6$. The bottom and top curves show the 95 per cent confidence region assuming a power law intrinsic alignment model with index $-3 < \alpha_{g+} < +1$. The center curve shows the contamination predicted by the best-fit parameters in Table 2.